Program Digest, 2019 IEEE International Ultrasonics Symposium (IUS)
Glasgow, Scotland, October 6-9, 2019

A global strain estimation algorithm for non-invasive vascular ultrasound elastography

Hongliang Li[1,2], Jonathan Porée[1,2], Boris Chayer[1], Marie-Hélène Roy Cardinal[1], Guy Cloutier[1,2,3]

[1]Laboratory of Biorheology and Medical Ultrasonics, University of Montreal Hospital Research Center, Montréal, QC, Canada;

[2]Institute of Biomedical Engineering, University of Montreal, Montréal, QC, Canada;

[3]Department of Radiology, Radio-Oncology and Nuclear Medicine, University of Montreal, Montréal, QC, Canada.

***Abstract*— Most strain estimation algorithms are window-based. Within a calculation window, cross-correlation or affine estimations are performed. However, there is always a trade-off between the window size, overlap and computation efficiency. We propose a parameterized affine model to estimate pixel-wise strain globally within the framework of the Horn-Schunck optical flow (OF) estimation, which enables to derive a global strain field efficiently without multiple windowed calculations. In addition, properties of the global pixel-wise estimation provide higher strain imaging resolution. Specifically, global strain fields were parameterized with discrete cosine transform (DCT) descriptions. A cost function including an OF constancy term, a smoothness constrain and a nearly incompressibility term was minimized to derive affine strain components (axial and lateral strains and shears), from which principal strains were determined. For the simulation study, the proposed method provided less estimation errors than the window-based Lagrangian speckle model estimator (LSME). The computation time with the proposed method was also reduced by more than 4 times compared with the LSME. For *in vitro* experiments, the proposed method was found to be able to detect a 1 mm hard inclusion.**

Keywords—optical flow, vascular ultrasound elastography, high resolution, sparse model

I. INTRODUCTION

Most strain estimation algorithms are window-based. Within a calculation window, cross-correlation [1-3] or affine [4-6] estimations are performed. Specifically, consecutive images are divided into overlapping windows. Assuming that motions of pixels within a window are uniform, window-based methods locally derive mean displacements and/or strains within that window. However, there is always a trade-off between window size, overlap and computation efficiency. For a given window size, a smaller overlap gives higher computation efficiency but a lower strain imaging resolution. Although a higher overlap results in a higher resolution, it would reduce computation efficiency and introduce worm artifact filtering [7].

This work was funded by the Collaborative Health Research Program of the Natural Sciences and Engineering Research Council of Canada (CHRP-462240-2014) and the Canadian Institutes of Health Research (CPG-134748). Authors acknowledge the scholarship support of the Québec Bioimaging Network of the Fonds de Recherche Québec Santé to Mr. Li.

An alternative way is to globally estimate pixel-wise motions in a region of interest (ROI) instead of using overlapping windows. Some approaches have been developed for quasi-static elastography [8-14], Doppler vector flow [15], myocardial motion tracking [16], [17] and computer vision [18]. Ones formulate pixel-based motion estimations as an optimization problem where a cost function incorporating a data term and a regularization term is minimized. However, this usually requires to optimize iteratively a cost function until convergence, which also impacts computation time. Moreover, these models only consider displacement or velocity fields and do not estimate strain directly. Additional spatial derivative is required to obtain strain. Such gradient operation enhances the variance of strain estimations when high frequency displacement noise is encountered. To our knowledge, a pixel-wise vascular strain estimator with an affine model considering all strain components without spatial derivatives on displacements has not yet been proposed.

In this study, we propose a parameterized affine model to estimate pixel-wise strain globally within the framework of the Horn-Schunck optical flow (OF) estimation, which enables to derive a global strain field efficiently without multiple windowed calculations.

II. ALGORITHM DESCRIPTION

A. Problem formulation

The proposed algorithm is within the framework of the Horn-Schunck (HS) optical flow method. A cost function incorporating a data term, a smoothness constraint and a nearly incompressibility constraint is minimized to derive motion fields,

$$\min\left\{\left\|\nabla I\cdot\vec{U}+I_t\right\|_2^2+\lambda_s\left(\left\|\mathrm{grad}(\nabla\cdot\vec{U})\right\|_2^2+\left\|\mathrm{grad}(\nabla\times\vec{U})\right\|_2^2\right)+\lambda_i\left\|\nabla\cdot\vec{U}\right\|_2^2\right\}. \quad (1)$$

The first term in (1) is from the optical flow constraint equation, where $\vec{U}=\{U_x,U_y\}$ is the displacement vector incorporating lateral displacement U_x and axial displacement U_y, respectively, I represents the image intensity, I_t denotes the

temporal gradient of the image intensity, and $\|\cdot\|_2$ stands for L2 norm. The second term is a two-order smoothness constraint to enforce the smoothness of the divergence and curl of the displacement field [19], [20], where $\nabla \cdot \vec{U} = \frac{\partial U_x}{\partial x} + \frac{\partial U_y}{\partial y}$, $\nabla \times \vec{U} = \frac{\partial U_y}{\partial x} - \frac{\partial U_x}{\partial y}$ are the divergence and curl of the displacement field, respectively, $\mathrm{grad}(\cdot)$ is the gradient operator, and λ_s is a regularization parameter to modulate the influence of the smoothness constraint. Since human arteries can be considered as nearly incompressible [21], we added a nearly incompressibility constraint in (1) as the third term. Here, λ_i is a regularization parameter to control the influence of the nearly incompressibility constraint. Similar incompressibility assumption has been used to improve the quality of strain estimations in the field of ultrasound strain imaging [5], [6], [22].

B. Regularized least squares estimation

Instead of solving the optimization problem of (1) using an iterative strategy as in the HS algorithm, we parameterized the displacement field using discrete cosine transform (DCT), then solved strain fields using a least squares method. Specifically, the displacement vector $\vec{U}$ of a pixel in an image of size $M \times N$ can be expressed with a linear combination of type-II discrete cosine basis functions as

$$\vec{U} = diag(B)c, \tag{2}$$

where $\{B\}_{M_t n+m} = \cos(k_x^m(2x+1))\cos(k_y^n(2y+1))$ denotes the DCT basis function vector with length $M_t N_t$, $k_x^m = \frac{m}{2M}\pi$, $k_y^n = \frac{n}{2N}\pi$, c represents DCT coefficients vector with length $2M_t N_t$, $diag(\cdot)$ defines a diagonal matrix, M_t, N_t stands for the size of the truncated discrete cosine coefficient (*i.e.,* $M_t \le M$, $N_t \le N$). Section III. C. justifies the choice of M_t and N_t. Putting (2) into (1), minimization of (1) is converted into the equation below:

$$\|\nabla I \cdot diag(B)c + I_t\|_2^2 + \lambda_s(\|\mathrm{grad}(\nabla \cdot diag(B)c)\|_2^2 + \|\mathrm{grad}(\nabla \times diag(B)c)\|_2^2) + \lambda_i\|\nabla \cdot diag(B)c\|_2^2 = 0. \tag{3}$$

For a given pixel coordinate, c is the only unknown variable in (3). Since c is with $2M_t N_t$ unknown DCT coefficients, we can globally consider all pixels in an image of size $M \times N$ to build an over-determined linear equation system to solve all DCT coefficients:

$$\boldsymbol{A}c = \boldsymbol{b}, \tag{4}$$

where $\boldsymbol{A} = \big(\nabla \boldsymbol{I} \cdot diag(\boldsymbol{B})\big)^T\big(\nabla \boldsymbol{I} \cdot diag(\boldsymbol{B})\big) + \lambda_s \mathrm{grad}\big(\nabla \cdot diag(\boldsymbol{B})\big)^T \mathrm{grad}\big(\nabla \cdot diag(\boldsymbol{B})\big) + \lambda_i \nabla \cdot diag(\boldsymbol{B})^T \nabla \cdot diag(\boldsymbol{B})$ and $\boldsymbol{b} = \big(\nabla \boldsymbol{I} \cdot diag(\boldsymbol{B})\big)^T \boldsymbol{I_t}$, $\{\boldsymbol{B}\}_{i,M_t n+m} = \cos(k_x^m(2x_i+1))\cos(k_y^n(2y_i+1))$, $\boldsymbol{I}$ and $\boldsymbol{I_t}$ represent the image intensities and temporal intensity gradients, respectively, of pixels in an image with size of $M \times N$.

Once DCT coefficients are estimated, U_x, U_y are determined using (2). Accordingly, strain components are represented by $S_{xx} = \frac{\partial U_x}{\partial x}$, $S_{xy} = \frac{\partial U_x}{\partial y}$, $S_{yy} = \frac{\partial U_y}{\partial y}$, $S_{yx} = \frac{\partial U_y}{\partial x}$, where S_{xx}, S_{xy}, S_{yy}, S_{yx} are lateral strain, lateral shear, axial strain and axial shear, respectively. Finally, the Cartesian strain components were combined and represented as principal minor and major strain tensors, ε_{min}, ε_{max}:

$$\varepsilon_{min,max} = \frac{S_{xx}+S_{yy}}{2} \pm \sqrt{\left(\frac{S_{xx}-S_{yy}}{2}\right)^2 + \left(\frac{S_{xy}+S_{yx}}{2}\right)^2}. \tag{5}$$

III. SIMULATIONS AND EXPERIMENTS

A. Simulations

A carotid artery model was created using COMSOL Multiphysics (Structural Mechanics Module, version 3.5, COMSOL, France). A soft necrotic core and four hard calcified inclusions were embedded in a medium mimicking a plaque. Displacements and strains of the vessel wall were computed using the finite element method (FEM). The ultrasound simulation program Field II [23] was used to obtain plane wave radiofrequency (RF) data considering 21 emission angles. The L14-5/38 linear array probe (Ultrasonix Medical Corporation, Richmond, BC, Canada) was simulated with a 7.2 MHz center frequency and a sampling rate of 40 MHz. RF data were beamformed using the delay-and-sum algorithm [24]. White Gaussian noise was added into beamformed images to make them more realistic with signal-to-noise ratios (SNR) of 20 dB.

The strain components were computed over consecutive frames from the simulated image sequence. The largest cumulated strain map as the final elastogram was determined using (5). To evaluate elastograms, the normalized root-mean-square-error (NRMSE) was used:

$$NRMSE = \frac{\sqrt{\frac{\sum_{i=1}^{N}(ref_i - est_i)^2}{N}}}{ref_{max} - ref_{min}}, \tag{6}$$

where N is the number of pixels in an elastogram, ref is the ground truth values, and est is the estimated values.

B. In vitro experiments

In vitro data from a soft phantom with a hard inclusion was used to evaluate the strain image resolution of the proposed algorithm. The soft background was made with 1% agar (A9799, Sigma–Aldrich Chemical, St Louis, MO), 4% gelatin (G2500, Sigma–Aldrich Chemical) and 95% distilled water. The hard inclusion of 1 mm was made with 15% polyvinyl alcohol, 3% cellulose particles (Sigmacell, type 5504, Sigma Chemical), and 82% distilled water that underwent 6 freeze-thaw-cycles.

External periodic vibrations were launched on the top of the phantom to induce axial compressions. RF data were acquired using a Sonix Touch ultrasonic system (Ultrasonix Medical Corporation, Richmond, BC, Canada) equipped with a L14-5/38 linear array. The same post-processing as considered in the simulation study was used to beamform plane wave data.

C. Parameters selection

To decide on values of λ_s and λ_i, we tested different pairs of these two parameters using simulation data. The chosen

parameter pair, $\lambda_s = 0.05$, $\lambda_i = 0.6$, provided the least NRMSE.

The thickness of the simulated carotid artery wall with a plaque was smaller than 3 mm. Thus, we determined the number of DCT coefficients, M_t or N_t, by the Cartesian grid resolution (lateral or axial) × image size (lateral M or axial N) / 1.5 mm to limit the minimum wavelength of the cosine basis function to 1.5 mm. The less DCT coefficients allowed the implementation of a least squares strategy as in (4). It also reduced the matrix size in (4) from $2MN$ to $2M_tN_t$, which reduced the computational complexity compared with a reconstruction with all DCT coefficients.

IV. RESULTS

A. The simulation study

Figure 1 shows elastograms of a simulated vascular phantom. The LSME estimator of [5], [6] was applied to compare with the proposed algorithm. The window parameters of the LSME were set to 1.0 mm × 1.0 mm window size and 80% overlap in axial and lateral directions. In the temporal direction, the time-ensemble number was 8 with 90% time overlap. The NRMSEs of principal minor strain maps with the LSME (fig. 1(c)) and proposed algorithm (fig. 1(e)) are 8.5% and 6.8%, respectively. For the principal major strain maps with the LSME and proposed algorithm, the NRMSEs are 9.6% and 7.0 %, respectively. Computation time with the LSME was 13.1 sec/frame, while the proposed method reduced speed by more than 4 times to 3.0 sec/frame.

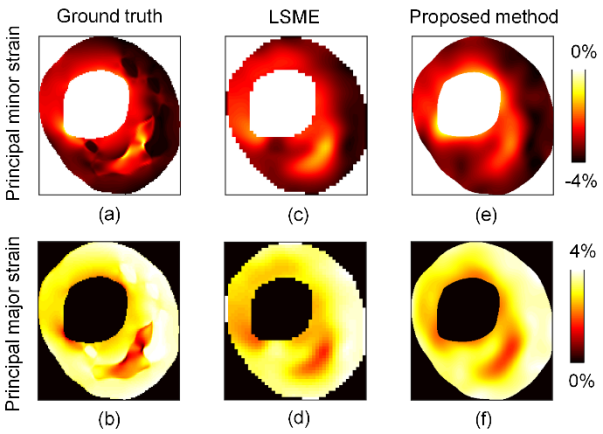

Fig. 1. Principal strain maps of a simulated vascular phantom with a soft inclusion and four hard inclusions. (a), (b) Ground truth. (c), (d) Principal strain maps with the LSME. (e), (f) Principal strain maps with the proposed method.

B. The in vitro experiment

Figure 2 presents results for imaging resolution test. The window overlap of the LSME was set to 99% to achieve pixel-wise image resolution. As seen in the axial strain map with the LSME (fig. 2(b)), worm artifacts attributed to correlation noise patterns due to a large overlap were noticed. On the other hand, the proposed method avoided these artifacts and allowed to detect a 1 mm hard inclusion where the LSME failed.

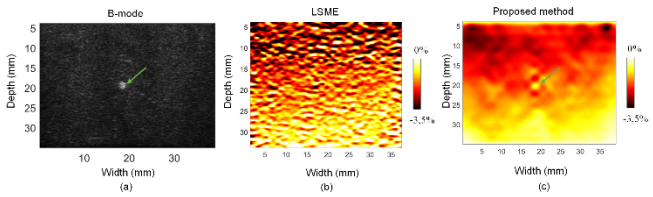

Fig. 2. (a) A soft phantom with a hard inclusion of 1 mm. (b) Axial strain with the LSME. (c) Axial strain with the proposed method.

V. CONCLUSION

In this paper, the proposed method provided more accurate strain estimations at high spatial resolution as well as computation efficiency. With simulation data, the proposed method gave less NRMSEs than with the LSME method. The computation time with the proposed method was also reduced by more than 4 times compared with the LSME. For the *in vitro* experiment, the proposed method avoided worm artifacts of window-based approaches and could detect a 1 mm hard inclusion.

VI. REFERENCES

[1] H. H. Hansen, R. G. Lopata, T. Idzenga, and C. L. de Korte, "Full 2D displacement vector and strain tensor estimation for superficial tissue using beam-steered ultrasound imaging," *Physics in Medicine & Biology,* vol. 55, no. 11, pp. 3201-3218, Jun 7 2010.

[2] S. Korukonda and M. M. Doyley, "Visualizing the radial and circumferential strain distribution within vessel phantoms using synthetic-aperture ultrasound elastography," *IEEE Trans Ultrason Ferroelectr Freq Control,* vol. 59, no. 8, pp. 1639-1653, Aug 2012.

[3] M. Larsson, B. Heyde, F. Kremer, L. A. Brodin, and J. D'Hooge, "Ultrasound speckle tracking for radial, longitudinal and circumferential strain estimation of the carotid artery-an in vitro validation via sonomicrometry using clinical and high-frequency ultrasound," *Ultrasonics,* vol. 56, pp. 399-408, Feb 2015.

[4] R. L. Maurice, M. Daronat, J. Ohayon, É. Stoyanova, F. S. Foster, and G. Cloutier, "Non-invasive high-frequency vascular ultrasound elastography," *Physics in Medicine and Biology,* vol. 50, no. 7, pp. 1611-1628, 2005.

[5] J. Poree, D. Garcia, B. Chayer, J. Ohayon, and G. Cloutier, "Noninvasive vascular elastography with plane strain incompressibility assumption using ultrafast coherent compound plane wave imaging," *IEEE Trans Med Imaging,* vol. 34, no. 12, pp. 2618-2631, Dec 2015.

[6] H. Li, J. Poree, M. H. Roy Cardinal, and G. Cloutier, "Two-dimensional affine model-based estimators for principal strain vascular ultrasound elastography with compound plane wave and transverse oscillation beamforming," *Ultrasonics,* vol. 91, pp. 77-91, Jan 2019.

[7] J. Ophir *et al.*, "Elastography: ultrasonic estimation and imaging of the elastic properties of tissues,"

Proceedings of the Institution of Mechanical Engineers, Part H: Journal of Engineering in Medicine, vol. 213, no. 3, pp. 203-233, 1999.

[8] E. Brusseau, J. Kybic, J. F. Deprez, and O. Basset, "2-D locally regularized tissue strain estimation from radio-frequency ultrasound images: theoretical developments and results on experimental data," *IEEE Trans Med Imaging,* vol. 27, no. 2, pp. 145-160, Feb 2008.

[9] H. Rivaz, E. M. Boctor, M. A. Choti, and G. D. Hager, "Real-time regularized ultrasound elastography," *IEEE Trans Med Imaging,* vol. 30, no. 4, pp. 928-45, Apr 2011.

[10] H. Rivaz, E. M. Boctor, M. A. Choti, and G. D. Hager, "Ultrasound elastography using multiple images," *Med Image Anal,* vol. 18, no. 2, pp. 314-329, Feb 2014.

[11] M. Omidyeganeh, Y. Xiao, M. O. Ahmad, and H. Rivaz, "Estimation of strain elastography from ultrasound radio-frequency data by utilizing analytic gradient of the similarity metric," *IEEE Trans Med Imaging,* vol. 36, no. 6, pp. 1347-1358, Jun 2017.

[12] H. S. Hashemi and H. Rivaz, "Global time-delay estimation in ultrasound elastography," *IEEE Transactions on Ultrasonics, Ferroelectrics and Frequency Control,* vol. 64, no. 10, pp. 1625-1636, 2017.

[13] M. Ashikuzzaman, C. J. Gauthier, and H. Rivaz, "Global ultrasound elastography in spatial and temporal domains," *IEEE Trans Ultrason Ferroelectr Freq Control,* vol. 66, no. 5, pp. 876-887, May 2019.

[14] Y. Zhang, S. Li, X. Li, H. Li, and H. Zheng, "A method of ultrasonic strain estimation under large tissue compression," *2013 IEEE International Conference on Medical Imaging Physics and Engineering,* pp. 158-161, 2013.

[15] M. Arigovindan, M. Suhling, C. Jansen, P. Hunziker, and M. Unser, "Full motion and flow field recovery from echo Doppler data," *IEEE Trans Med Imaging,* vol. 26, no. 1, pp. 31-45, Jan 2007.

[16] N. Ouzir, A. Basarab, H. Liebgott, B. Harbaoui, and J. Y. Tourneret, "Motion estimation in echocardiography using sparse representation and dictionary learning," *IEEE Trans Image Process,* vol. 27, no. 1, pp. 64-77, Jan. 2018.

[17] N. Ouzir, A. Basarab, O. Lairez, and J. Y. Tourneret, "Robust optical flow estimation in cardiac ultrasound images using a sparse representation," *IEEE Trans Med Imaging,* vol. 38, no. 3, pp. 741-752, Sep 18 2019.

[18] B. K. P. Horn and B. G. Schunck, "Determining optical flow," *Artificial intelligence,* vol. 17, no. 1-3, pp. 185-203, 1981.

[19] T. Rohlfing, C. R. Maurer, Jr., D. A. Bluemke, and M. A. Jacobs, "Volume-preserving nonrigid registration of MR breast images using free-form deformation with an incompressibility constraint," *IEEE Trans Med Imaging,* vol. 22, no. 6, pp. 730-741, Jun 2003.

[20] T. Corpetti, É. Mémin, and P. Pérez, "Dense estimation of fluid flows," *IEEE Transactions on pattern analysis and machine intelligence,* vol. 24, no. 3, pp. 365-380, 2002.

[21] A. Karimi, T. Sera, S. Kudo, and M. Navidbakhsh, "Experimental verification of the healthy and atherosclerotic coronary arteries incompressibility via Digital Image Correlation," *Artery Research,* vol. 16, pp. 1-7, 2016.

[22] H. Li, J. Porée, and G. Cloutier, "A modified affine phase-based estimator for noninvasive vascular ultrasound elastography using coherent plane wave compounding and transverse oscillation imaging," *IEEE International Ultrasonics Symposium,* pp. 1-4, 2016.

[23] J. A. Jensen, "Field: A program for simulating ultrasound systems," *Medical & Biological Engineering & Computing,* vol. 34, no. 1, pp. 351-353, 1996.

[24] G. Montaldo, M. Tanter, J. Bercoff, N. Benech, and M. Fink, "Coherent plane-wave compounding for very high frame rate ultrasonography and transient elastography," *IEEE Transactions on Ultrasonics, Ferroelectrics and Frequency Control,* vol. 56, no. 3, pp. 489-506, 2009.